Energy 282 (2023) 128373

Contents lists available at ScienceDirect

Energy

journal homepage: www.elsevier.com/locate/energy

# A methodology for cost-effective analysis of hydrokinetic energy projects

D.M. Fouz [a], R. Carballo [a,*], I. López [a], X.P. González [a], G. Iglesias [b,c]

[a] Departamento de Enxeñaría Agroforestal, Universidade de Santiago de Compostela, EPSE, Rúa Benigno Ledo s/n, 27002, Lugo, Spain
[b] School of Engineering and Architecture & MaREI, Environmental Research Institute, University College Cork, Ireland
[c] School of Engineering, Computing and Mathematics, University of Plymouth, UK

ARTICLE INFO

Handling Editor: Soteris Kalogirou

*Keywords:*
Tidal stream
Tidal energy
Marine renewable energy
Offshore renewable energy
Cost model
Energy production model

ABSTRACT

The cost-effective analysis (CEA) of hydrokinetic farms is typically based on simplistic assumptions regarding the performance and cost structure of hydrokinetic energy converters (HECs) and, in consequence, may lead to ill-informed decision-making. In this work, a novel approach to selecting the most appropriate combination of HEC and site within a coastal area is developed, with the accurate computation of the CEA parameters as the cornerstone. The approach, which is illustrated through a case study in the Shannon Estuary (W Ireland), encompasses four models, namely: (i) HEC-site selection model, (ii) energy production model, (iii) CAPEX model, and (iv) OPEX model. By avoiding simplistic assumptions, the proposed approach improves on current procedures and enables developers to accurately compute any cost-effective parameter of interest. In particular, operation and maintenance costs are considered, along with economies of scale, which are typically disregarded in existing procedures. Beyond the interest of the results of the Shannon case study, the approach can be implemented in other regions with potential for hydrokinetic energy conversion.

## 1. Introduction

Coastal areas have supported human activity throughout history in many different ways. In the socioeconomic sphere, these areas have been traditionally used for transport and food supply [1,2]. As a result of the increased public awareness of environmental issues, protected or conservation areas (e.g., Natura 2000) have emerged alongside traditional socioeconomic activities, which have grown significantly (e.g., tourism or heritage) [3,4]. This is also the case of marine renewable energy exploitation, which is posited as a new, promising coastal use [5–12].

Within the different types of marine renewable energies, hydrokinetic energy, primarily resulting from the tide (e.g. Ref. [13]), reinforced in some coastal areas by river discharges and density gradients (e.g. Ref. [14]), is expected to attain a commercial stage in the forthcoming years [15]. The exploitation of this resource is carried out by means of hydrokinetic energy converters (HECs), of which different types exist with varying degrees of technological maturity. Turbine-based solutions, and in particular horizontal axis turbines, are considered to be approaching the commercial stage [16–18]. The state-of-the-art third-generation HECs are designed to operate with relatively low cut-in velocities (i.e., 0.7–1.0 m/s) [19,20].

As a consequence of this heterogeneity in technological maturity, reliable metrics should be developed to accurately assess the technical and economic viability of hydrokinetic energy projects in decision-making processes. As a first approach to technical viability, the Technology Readiness Level (TRL) is usually mentioned as a standard or a metric-based model with several applications in R&D activities, such as the development of HECs [21,22]. However, in order to reduce the uncertainties of hydrokinetic energy projects and ensure their economic viability, the TRL model should be complemented by a cost-effective analysis (CEA), which provides metrics (e.g., LCOE, NPV, IRR) describing the techno-economic performance of technologies under development or proposed projects [23].

The estimation of CEA parameters is usually based on simplified methods, considering either their spatial distribution or, in a simpler approach, delocalised approximations [24]. The main weakness of these approaches is their unrealistic cost structure, which may produce misleading results. In the case of tidal energy projects, the resulting figures typically lack accuracy, which may be seen as a direct consequence of the limitations of the procedure applied, namely [25]: (i) performance computation based on limited and non-reliable HEC data, (ii) consideration of the different economic aspects in terms of expected percentage over the total investment, or (iii) disregard for specific

* Corresponding author.
*E-mail address:* rodrigo.carballo@usc.es (R. Carballo).

https://doi.org/10.1016/j.energy.2023.128373
Received 1 February 2023; Received in revised form 11 May 2023; Accepted 7 July 2023
Available online 15 July 2023

aspects, which contributes significantly to real costs. Another aspect closely related to the computation of CEA parameters is the selection of the sites or areas to be subject to this analysis. This selection is typically based merely on the available energy resource [26–28]. In a few cases, a reduced number of geomorphological parameters (e.g., water depth) have also been taken into account [29,30]. Notwithstanding the interest of these methods for a preliminary selection of coastal areas, additional information (e.g., socioeconomic) needs to be considered in more advanced stages. In effect, an appropriate site-selection should also consider aspects such as the coexistence of the energy exploitation with other marine uses, or the site-specific costs of installation and operation [31,32].

In this context, it is important to remark that miscalculated CEA figures may result from not accurately considering specific aspects of cost analysis, such as the operation costs, or from neglecting potential cost reductions through economies of scale [33]. In the case of large coastal areas, the application of the current procedures could result in overly homogeneous CEA figures, as the spatial variability of the energy resource over short distances is not usually accounted for in the computation of these metrics (low to mid resolution energy resource models) [34].

In this research, a novel approach for accurately computing the CEA parameters of hydrokinetic energy projects is developed, leading to a significant improvement with respect to currently available methods. The proposed approach addresses the major difficulties and uncertainties when computing the main aspects affecting the CEA of hydrokinetic energy farms, avoiding simplistic and unreliable assumptions, and improving on current procedures. Thus, the implementation of this novel procedure will lead to the selection of the optimum HEC-site combination for installing a hydrokinetic farm in a coastal area.

The novelty of this work lies in the consideration of the following aspects: (i) the energy production, which is assessed by combining high-resolution numerical modelling results with spatial analysis algorithms; (ii) the installation costs, whose breakdown in terms of unitary costs is thoroughly analysed, including the effects of economies of scale; (iii) the operation costs, which are computed by means of an ad hoc Operation and Maintenance (O&M) model, including several operational parameters and strategies.

Other aspects dealing with the energy transmission or storage related to the specific characteristics of the electrical grid, or the integration with short-term energy storage to help balance the local demand with the varying supply typical of hydrokinetic and tidal farms, are outside the scope of the present work and require specific research [35–40].

The proposed procedure to develop the CEA of hydrokinetic energy projects is applied, for the first time, to a specific case study in the Shannon Estuary (W Ireland) (Fig. 1) and computed in terms of Levelized Cost of Energy (LCOE). Preliminary studies have recognised the potential of this area for hydrokinetic energy exploitation [41,42]. Previous works fully described the hydrokinetic energy resource in the Shannon Estuary, identifying a number of areas as of particular interest [30]. More recent studies highlighted the energy potential of Tarbert Area in the middle estuary (Figs. 1 and 2) by considering: (i) the exploitable resource, (ii) the costs of installation, and (iii) the socio-economic and environmental pre-existent activities [31,43,44]. The integration of these aspects led to the computation of the Integrated Hydrokinetic Energy (IHE) index and, on this basis, to the delimitation of a large area in the surroundings of Tarbert (≈3 $km^2$) (Fig. 2) with the highest potential, with a value of IHE = 4.15 (being IHE = 1 the suitability threshold for hydrokinetic energy exploitation). In the present work, this region is retained as a case study for defining the best HEC-site combination by applying the proposed procedure.

This paper is structured as follows. In Section 2, a brief overview of the proposed methodology used to compute the CEA is presented. Next, in Section 3, the tools for defining feasible HEC-site combinations are introduced and implemented to the area of interest. Afterwards, the main aspects considered for CEA computation are defined, and the results from its application summarized: (i) energy production (Section 4), (ii) capital expenditures, CAPEX (Section 5), and (iii) operational expenditures, OPEX (Section 6), In Section 7, the integration of results and CEA computation is conducted for the Tarbert Area, and the results compared with available state-of-the-art methodologies. Finally, the major conclusions to this work are depicted in Section 8.

## 2. General description of the procedure

The main objective of this work is to define and apply a new approach to accurately conduct a cost-effective analysis (CEA) of hydrokinetic energy farms, considering all the aspects involved in the process, and thus leading to the identification of the best HEC-site combination within a coastal area.

The proposed approach consists of five steps:

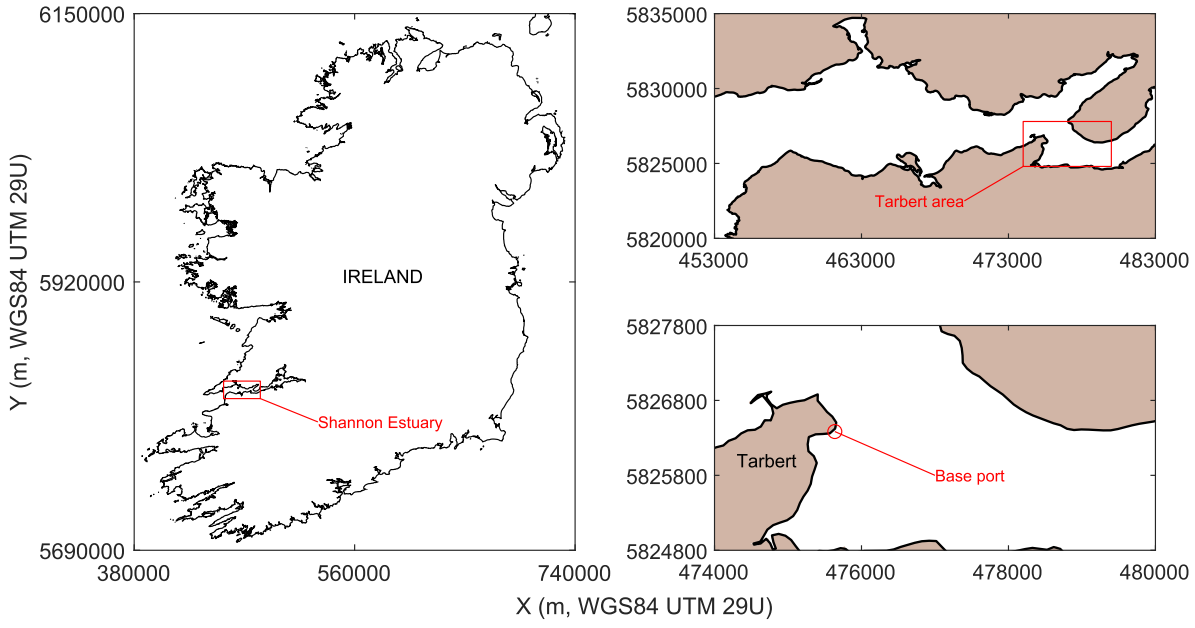


**Fig. 1.** Location of Shannon Estuary in W Ireland pinpointing Tarbert Area.

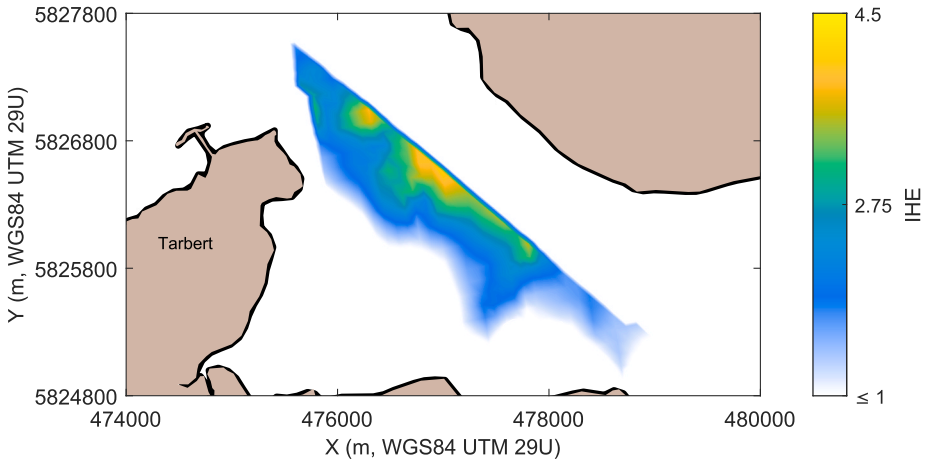


**Fig. 2.** IHE index over the exploitable threshold (IHE ≥1) in the Tarbert Area.

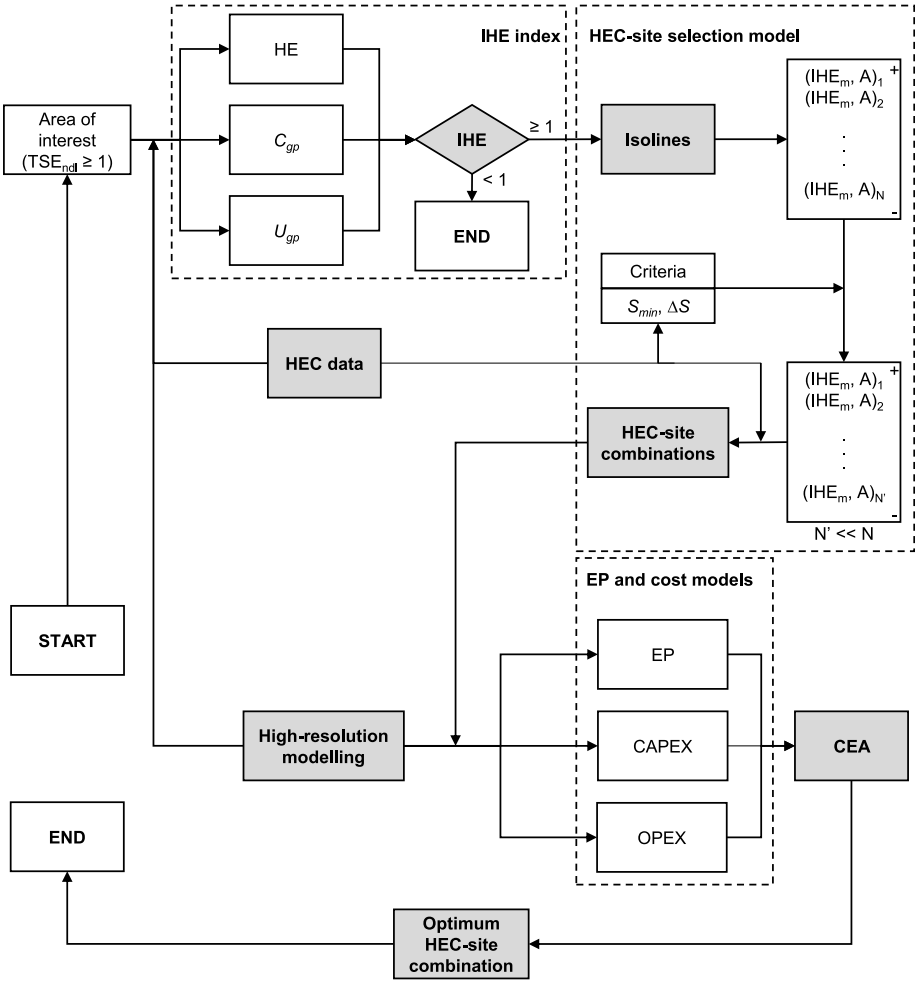


**Fig. 3.** Flowchart of the proposed procedure.

(i) The development of an HEC-site selection model (Section 3), which employs the IHE index and spatial analysis algorithms to define different HEC-site combinations, allowing for economies of scale by analysing various farm sizes based on specific criteria (Section 3).
(ii) The application of an energy production model leading to the computation of the Annual Energy Production (AEP) of the different HEC-site combinations previously defined, based on high-resolution numerical modelling.
(iii) The definition of a Capital Expenditures (CAPEX) model (Section 5), which is based on a detailed breakdown in unitary costs and an ad hoc algorithm for assessing the effects of the economies of scale resulting from the different farms analysed.
(iv) The definition of an Operational Expenditures (OPEX) model (Section 6), considering HEC-specific O&M procedures, including

the analysis of human and material resources and the definition of specific weather windows.

(v) The integration of previous results (ii to iv) to provide reliable CEA parameters for the different HEC-site combinations, leading to the selection of the best alternative.

For the sake of clarity, a flowchart of the procedure is provided in Fig. 3.

This procedure is illustrated through a case study in the Tarbert Area of the Shannon Estuary (Ireland) [30,31,41,42]. The CEA is carried out in terms of Levelized Cost of Energy (LCOE) – a metric widely used in marine renewable energy projects, including for the selection of sites for hydrokinetic energy farms [24–27,45,46].

## 3. HEC-site selection model

The first step of the proposed approach is the definition of all the feasible HEC-site combinations. This is a key stage upon which depend several parameters that influence the cost structure (inter alia, the final layout of the farm or maintenance strategies), including the possible effects of the economies of scale and the performance of the plant and, in consequence, the resulting CEA values.

With the aim of generalizing the results provided, generic taxonomies of energy converters are considered (Section 3.1), including information about their reliability, which will be retained for its use in further sections. As regards locations, the results of the IHE index in the surroundings of Tarbert are used as a starting point for the definition of different areas with homogeneous levels of energy resource, which are processed to identify the suitable areas under specific criteria by means of spatial analysis algorithms (Section 3.2).

### 3.1. Characteristics and reliability of the energy converters considered

The present work aims to provide results as accurate and realistic as possible in a nascent research field, hydrokinetic energy exploitation. As mentioned above, only horizontal-axis turbine-based devices are approaching commercial maturity, resulting in a lack of reliable economic information of HECs. In order to overcome these limitations, it is usual to resort to general taxonomies of HECs, grouping generic designs with a certain homogeneity, especially in the field of reliability, where surrogate data can be easily available from other renewables (e.g., wind energy). Likewise, despite the assumptions made, this approach is helpful to provide accurate figures of the cost structure of HECs and, in particular, of their costs of installation (Section 5), primarily due to the possibility of complementing their breakdown by means of different data sources, which are assumed to be common or scalable for the whole taxonomy considered [47].

Horizontal-axis turbines are usually classified depending on their seabed fixing as [48]: (i) bottom-fixed and (ii) floating devices. This division is connected with the available water depth and, in consequence, with the diameter of the turbine. Monopile bottom-fixed gravity foundations are usually prescribed up to 20–30 m depth, and floating, moored solutions for deeper areas [31]. This general picture is similar to offshore wind energy facilities, allowing us to use surrogate data to compute accurate reliability figures for HECs under an assembly or subassembly approach. The reader is referred to Ref. [47] for further information about this approach and its procedures.

Therefore, in order to select generic energy converter designs, representative of the aforementioned taxonomies and covering the most common horizontal-axis turbines and a wide range of diameters, two different HECs are considered: (i) a floating device of 4.5 m of diameter (F-HEC), which in turn could be applied to most of the areas of interest for hydrokinetic energy exploitation, and (ii) a bottom-fixed converter of 16 m of diameter (BF-HEC), which is of interest in a large number of non-depth limited coastal areas, such as deep estuaries. The main characteristics of the HECs selected, along with their reliability data in terms of average annual number of reparations required, which are retained for its use in further sections, are summarized in Table 1.

### 3.2. Selection of areas for CEA

Previous works have highlighted the energy potential of the Tarbert Area by considering not only its hydrokinetic energy resource, but also its morphological configuration, by applying the $TSE_{ndl}$ index [30], along with socioeconomic and environmental aspects, through the implementation of the IHE index [31]. On the basis of the application of the IHE index, a large area of approx. 3 $km^2$ with values above a minimum threshold of IHE = 1 (i.e., the threshold value of the IHE indicating suitability for hydrokinetic energy exploitation) has been delimited. The definition of suitable smaller areas for energy exploitation requires to take into account the spatial variability of the available resource within this large area; in fact, within it, the maximum value of the IHE index, IHE = 4.15, is roughly two times higher than its mean value, IHE = 2.10 [31]. The more reduced the area, the greater the IHE index; however, the larger the area considered, the higher the number of HECs, which would result in a cost reduction as a consequence of the economies of scale, not considered in the IHE index. With the aim of defining suitable areas for hydrokinetic energy exploitation considering this spatial variability of the energy resource and the resulting effects on the economies of scale, a complex spatial analysis algorithm (Fig. 3) is developed and applied to the Tarbert Area as follows.

First, the entire region delimited by the isoline IHE = 1 is subdivided into several sub-areas or polygons by considering isolines of a value ranging from 1 to the maximum value of the IHE index within the whole area by considering a given step. In the present application, a step of 0.2 is proposed; however, this value can be adapted based on the specific characteristics of the site. Second, the mean value of the IHE index at each polygon is computed along with their total surface. Third, the polygons subsequently obtained are rearranged according to their value of mean IHE index in decreasing order (i.e., increasing their total available surface). Finally, some of the polygons obtained are retained for further analysis from the rearranged list. To this end, the selection procedure considers the following criteria, being applied from the top to the bottom of the list.

The polygons to be retained must fulfil simultaneously two criteria: (i) to have, at least, a minimum total surface, $S_{min}$, and (ii) to provide a significant relative increase in the total available surface, $\Delta S$, with respect to the preceding selected polygon in the list. In the present work, these values are established as follows [27,49–54]: $S_{min} = 5$ $hm^2$ and $\Delta S = 100\%$. This second criterion allows us to consider the effects of economies of scale on the cost structure of the hydrokinetic farm.

### 3.3. Application of HEC-site selection model

The results of the application of the proposed HEC-site selection model to the Tarbert Area in the Shannon Estuary are provided in Figs. 4 and 5.

In Fig. 4, the different polygons obtained by considering isolines of a value ranging from IHE = 1 to the maximum value of the IHE index by considering a step = 0.2 are plotted (in black). Likewise, in order to facilitate the understanding of the results and of the proposed HEC-site selection model, additional isolines with step = 0.6 are also plotted (colour code). A total of 30 polygons are apparent. Finally, as result of the application of the rest of the procedure and the surface criteria given by $S_{min} = 5$ $hm^2$ and $\Delta S = 100\%$, in Fig. 5 the polygons retained are plotted. Only five polygons resulting from this procedure are considered for further analysis (A to E), allowing the consideration of the effects of economy scale. In addition, the polygon IHE = 1 is also retained. Their main characteristics are presented in Table 2.

Based on the characteristics (water depth) of the areas selected, and the characteristics of the selected devices (i.e., surface occupied per unit of HEC and minimum water depth required) (Table 1), a total of seven

**Table 1**
Main technical characteristics and reliability data of the HECs considered [rotor diameter (Ø), swept area ($A$), minimum water depth ($d_{min}$), total surface in plan view occupied per each device ($S_{unit}$), cut-in velocity ($V_{ci}$), rated velocity ($V_r$), cut-off velocity ($V_{co}$), rated power ($P_r$), power coefficient in normal operation ($C_{pNO}$), power coefficient in stall control ($C_{pSC}$), failure rate ($\lambda$)].

| HEC | Ø (m) | $A$ (m$^2$) | $d_{min}$ (m) | $S_{unit}$ (m$^2$) | $V_{ci}$ (m/s) | $V_r$ (m/s) | $V_{co}$ (m/s) | $P_r$ (kW) | $C_{pNO}$ | $C_{pSC}$ | $\lambda$ (no/yr) |
|---|---|---|---|---|---|---|---|---|---|---|---|
| BF-HEC | 16.00 | 200.00 | 25.00 | 1920.00 | 1.00 | 2.50 | 3.10 | 1200.00 | 0.48 | n.a. | 4.54 |
| F-HEC | 4.50 | 15.90 | 7.00 | 760.00 | 0.70 | 2.70 | 3.75 | 56.00 | 0.35 | 0.20 | 5.37 |

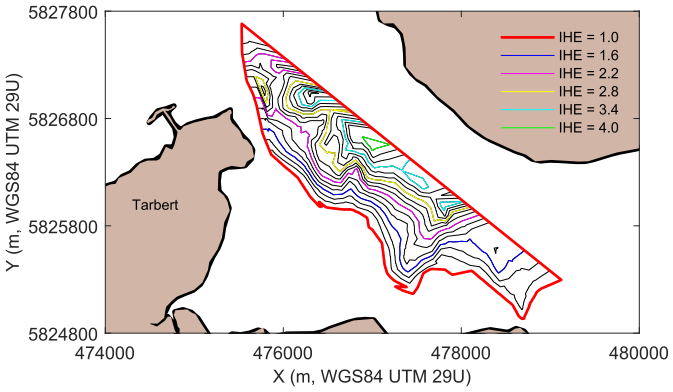


**Fig. 4.** Isolines of the IHE index (0.2 of step for isolines in black and 0.6 for isolines with colour code) within polygon IHE = 1. (For interpretation of the references to colour in this figure legend, the reader is referred to the Web version of this article.)

HEC-site combinations are retained for further CEA: F-HEC can be installed within polygons A to E and IHE = 1; in the case of BF-HEC, it can operate only within polygon E.

## 4. AEP model

### 4.1. Model description

Once defined the different HEC-site combinations resulting from the methodology described in Section 3, the next step in order to assess the techno-economic performance of these combinations is to accurately quantify their annual energy production (AEP). To this end, a high-resolution numerical model (Delft3D-FLOW) of the Shannon Estuary is implemented (in its 2DH form) and successfully validated, allowing the simulation of its hydrodynamics during a complete year [55–57]. For further details about the implementation and validation of the numerical model the reader is referred to Refs. [30,31]. Once the hydrodynamics of this coastal area are fully described in spatiotemporal terms, the electric energy production, $E_e$, of a HEC operating during a period of time $T$ can be computed as follows [58]:

$$E_e = \frac{AC_p\rho}{2}\int_{t=0}^{t=T}[V(t)]^3 dt, \quad (1)$$

where $A$ represents the turbine swept area, $C_p$ is the power coefficient which models the efficiency of the HEC selected, $\rho$ stands for the water density and $V(t)$ is the instantaneous vertically averaged flow velocity.

However, an accurate computation of this energy production in a

**Table 2**
Main characteristics of the sites selected [mean value of the IHE index ($IHE_m$), standard deviation ($\sigma$), mean water depth ($h_m$), surface ($S$), distance between the centroid of the polygon and the base port ($d_{C\text{-}BP}$)].

| Polygon | $IHE_m \pm \sigma$ | $h_m \pm \sigma$ (m) | $S$ (hm$^2$) | $d_{C\text{-}BP}$ (km) |
|---|---|---|---|---|
| A | 3.93 ± 0.08 | 9.22 ± 1.09 | 8.26 | 1.36 |
| B | 3.74 ± 0.20 | 10.00 ± 1.68 | 18.37 | 1.38 |
| C | 3.43 ± 0.30 | 12.02 ± 2.96 | 46.32 | 1.54 |
| D | 3.11 ± 0.43 | 14.34 ± 3.69 | 99.17 | 1.30 |
| E | 2.53 ± 0.66 | 17.21 ± 5.00 | 208.96 | 1.26 |
| IHE = 1 | 2.15 ± 0.80 | 16.97 ± 5.07 | 297.97 | 1.48 |

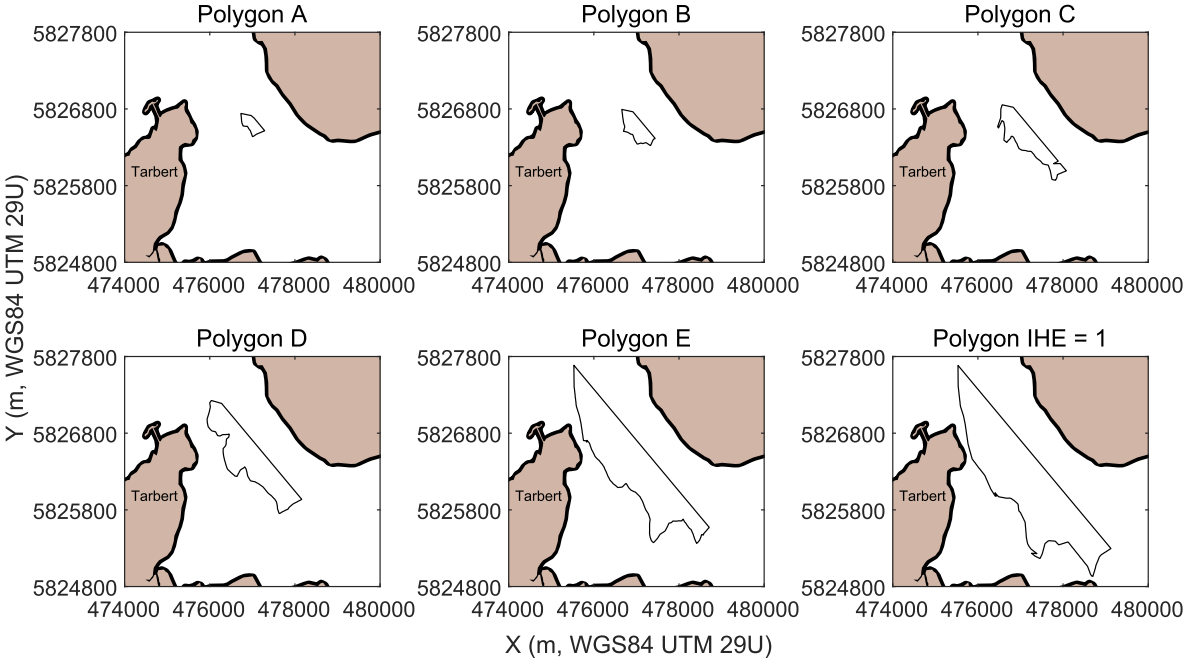


**Fig. 5.** Delimitation of the resulting polygons (A to E), along with polygon IHE = 1.

large coastal region, as is the case of the Tarbert Area, is not straightforward. Given the heterogeneity in terms of available surface of the different sub-areas or polygons of interest selected in Section 3, the spatial variability of the energy resource could result in inaccurate figures of energy production. To avoid this issue, a specific procedure is defined in order to compute the energy production of the different HEC-site combinations. Thus, the site-specific hydrodynamic regime of each polygon considered has been reconstructed based on high-resolution numerical results as follows: for each time step of the numerical simulation, the computed values of flow velocity of each grid cell contained in the polygon considered are averaged, constituting a site-specific and time-dependent hydrodynamic regime for each polygon analysed. So, the characteristic velocity at each polygon at each time step, $V_c$ ($t$), can be computed as:

$$V_c(t) = \frac{1}{n}\sum_{i=0}^{i=n} V_c(i), \tag{2}$$

where $i$ and $t$ represent the numerical cell number and time step, respectively. Thus, the characteristic mean velocity at each polygon, $V_c$, can be computed as:

$$V_c = \frac{1}{T}\sum_{t=0}^{t=T}\left[\frac{1}{n}\sum_{i=0}^{i=n} V_c(i,t)\right], \tag{3}$$

in this way, the energy production of the different HEC-site combinations can be accurately computed, including the effects of the spatial variability of the energy resource, by combining the time distribution of the characteristic velocity, $V_c$ ($t$), with the characteristics of each HEC considered (Table 1) by means of Eq. (1).

### 4.2. Application of AEP model

The results of the application of the proposed AEP model to the Tarbert Area are provided in Figs. 6 and 7.

In Fig. 6, the resulting time distribution of the characteristic velocity during a complete annual year at each polygon is shown. As a result of these time distributions, the following characteristic mean velocities, $V_c$, are attained: 1.20 m/s, 1.05 m/s, 1.16 m/s, 1.12 m/s, 1.03 m/s and 0.98 m/s for polygons A, B, C, D, E, and IHE = 1, respectively.

In Fig. 7, the figures of AEP and capacity factor ($C_f$) for the different HEC-site combinations retained are plotted. AEP is computed by combining the site-specific hydrodynamic regime and the power curve of the HECs considered as provided by the device developers. $C_f$ is obtained according to Ref. [59].

It can be observed that the polygon where F-HEC produces the largest amount of energy is that with the largest surface, IHE = 1 with 174.7 GWh, progressively reducing its energy production as the surface reduces: polygons E with 148.0 GWh, D with 89.9 GWh, C with 45.2 GWh, B with 14.3 GWh, and A with 8.9 GWh. In the case of BF-HEC, its annual energy production in polygon E is 45.1 GWh. This is the result of the significantly larger number of devices in the larger polygons (at least 100% of increase in the total surface with respect the preceding polygon according to the established criteria), which does not indicate a better performance. In fact, the smaller the polygons, the higher their IHE, and therefore the performance in terms of $C_f$ could tend to be the opposite. In the case of F-HEC: polygons A with 16.84%, B with 12.07%, C with 15.12%, D with 13.89%, E with 10.95% and IHE = 1 with 9.28%. In the case of BF-HEC, its $C_f$ in polygon E is 8.42%. This expected tendency does not apply to all cases, e.g. polygon B, given that IHE index also considers, in addition to the energy resource, the total costs although in

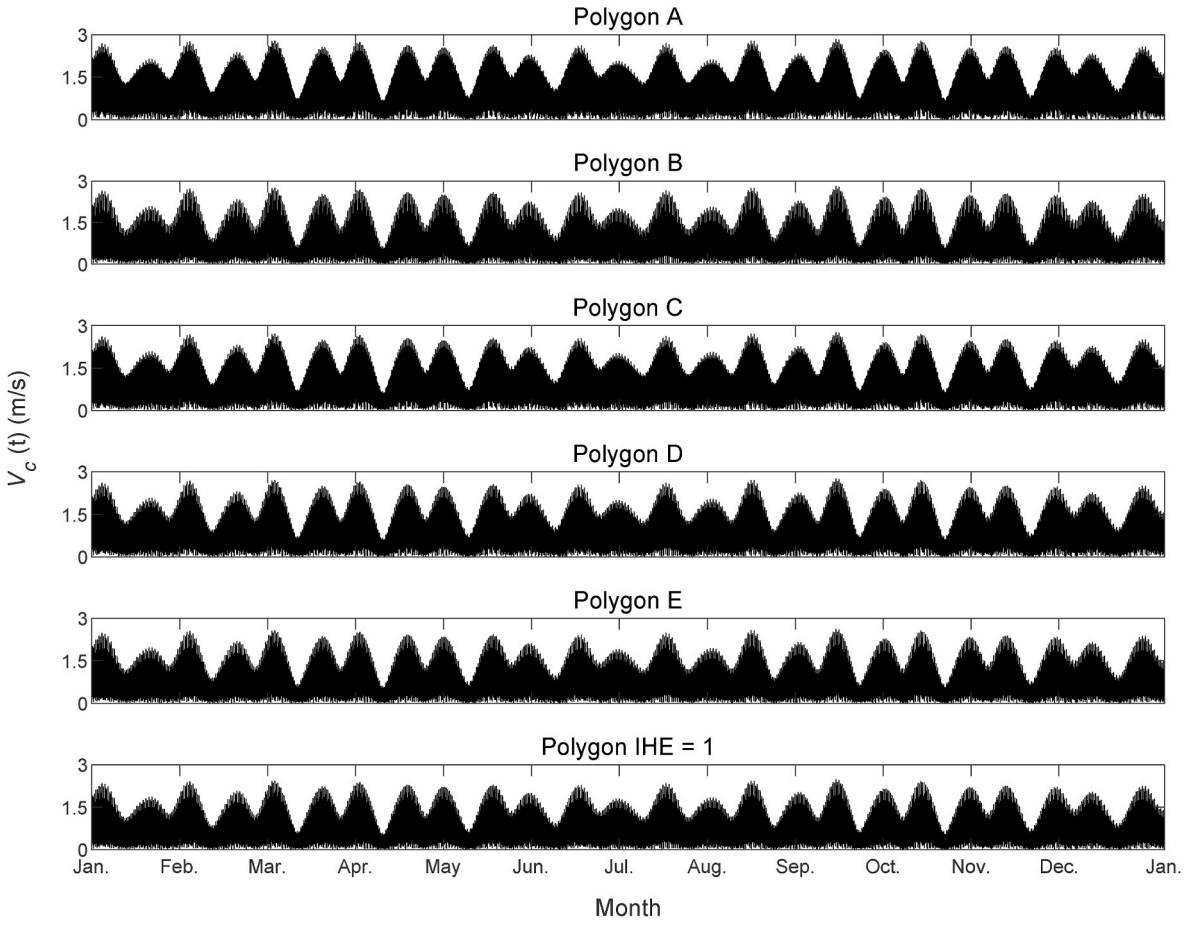


**Fig. 6.** Time distribution of the characteristic velocity, $V_c$ ($t$), in the selected polygons.

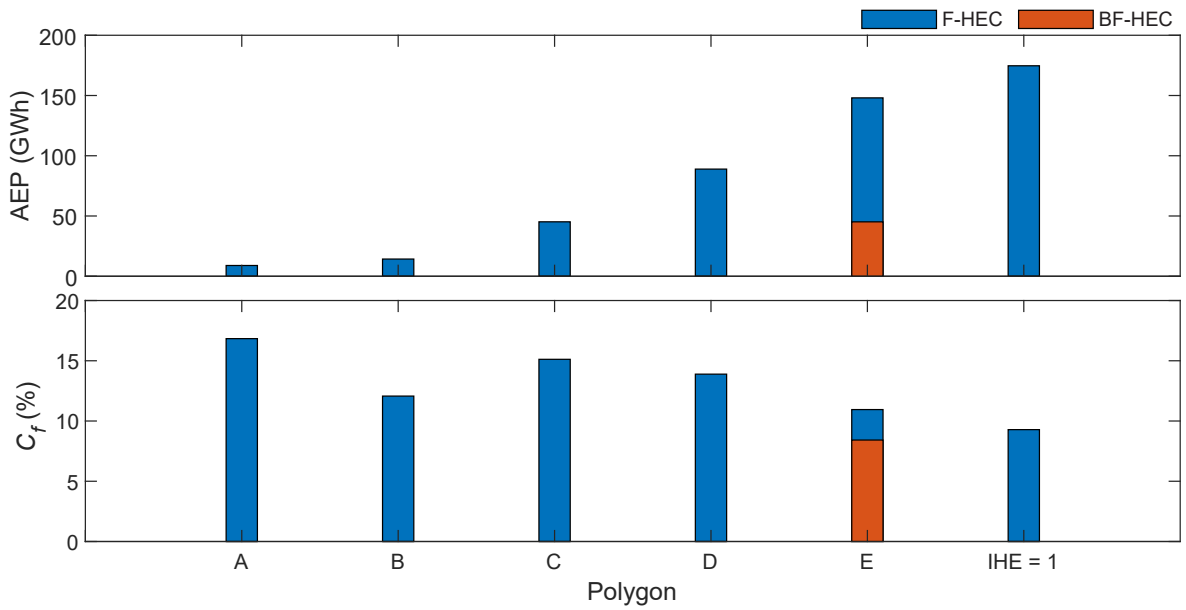


**Fig. 7.** AEP (above) and $C_f$ (below) for the selected HEC-site combinations.

a more simplified way than that proposed in the present work.

## 5. CAPEX model

### 5.1. Fundamentals of CAPEX estimation

CAPEX stand for the capital expenditures needed for the installation, in the present case, of a hydrokinetic farm. They are usually considered as a one-off expenditure, usually incurred in the first year of the project or in the first payment period (prior to the beginning of the operation of the farm). In consequence, CAPEX group all the construction costs of the plant, commonly representing more than 70% of its total expenses [45]. As a result of their economic magnitude, and in order to make available an accurate assessment of CAPEX, it is necessary to define in detail their cost items and structure, for which a widely used unitary costs model should be defined (Section 5.1) and subsequently implemented (Section 5.2) to compute the CAPEX of the different HEC-site combinations defined in Section 3 — instead of a global percentage, which might produce misleading results.

CAPEX is usually broken down into three cost categories [60]: (i) management and engineering costs ($CAPEX_1$), which encompasses the cost of different planning activities needed to ensure the viability of the project and the fulfilment of all its technical requirements (e.g., conceptualization, design, quality management, etc.); (ii) manufacturing costs ($CAPEX_2$), including the cost of the main structural elements of the farm and its equipment (e.g., devices, cabling, foundations or moorings, etc.); and (iii) installation costs ($CAPEX_3$), which include, among others, the expenses of the deployment and grid connection of the plant. The evaluation of these cost categories in the proposed model is explained in detail in Section 5.2.

### 5.2. Definition of CAPEX model

An accurate computation of $CAPEX_1$ to $CAPEX_3$ terms is a key point to develop the CEA of a hydrokinetic farm, especially in the case of $CAPEX_2$, which has been estimated at about 80% of the total CAPEX [45,61]. However, this value is highly dependent on the characteristics of the farm and should be accurately computed for each specific project. In this context, the only way to obtain realistic CAPEX figures is, as in the case of a conventional engineering project, to assess them by means of measurements and unitary costs. The definition of these data requires a detailed design of the HEC, e.g., through CAD tools [62], and a reliable breakdown of unitary costs, which is not typically available in the literature. To this end, the use of HEC types and representative generic designs are required.

In the present application, a detailed and validated unitary costs model [60,63–65] has been used by combining its breakdown (Table 3) with the specific measurements of the HECs considered, according to their significative taxonomic similarities. For further details about this model and its implementation, the reader is referred to Ref. [60].

Likewise, the present CAPEX model also considers the effects of the economies of scale resulting from the consideration of different farm sizes for installing the selected HECs, for which and ad hoc algorithmic procedure is applied. This procedure is based on a detailed analysis of the farm size (as a function of the installed power, $P$) and its influence on CAPEX figures for a wide range of proposed hydrokinetic plants, ranging from reduced plants, e.g., 0.5 MW [66], which were planned for the self-sufficiency of local facilities, to large offshore farms, e.g., 50 MW, with remarkable similarities with wind farms [25]. In this context, an increase in the number of HECs may lead to a considerable reduction in the costs in the case of initially proposed small to medium farm sizes; however, as the size of the farm grows, the increase in these effects progressively reduces up to a point at which are maximum [33]. In the present work, these limits have been widely analysed in terms of installed power in tidal energy and other renewables — for farms with installed power over approx. 30 MW the CAPEX presents maximum reductions of about 35% [67–69]. Moreover, as previously established, this reduction is more abrupt in the case of increasing the size of small farms than when approaching the aforementioned limit (i.e., 30 MW), which could be represented through a logarithmic function [70]. Based on these considerations, and by applying a parametric analysis to several hydrokinetic farms within a wide range of installed power (i.e., 0.5–50 MW), the effects of the economies of scale in terms of CAPEX reduction can be computed for hydrokinetic farms below 30 MW as follows:

$$CAPEX_{red}(\%) = 100 \times [8.4805 \ln(P) + 5.8782]. \quad (4)$$

Above this limit the CAPEX reduction would be set as a constant (35%).

### 5.3. Application of CAPEX model

The results of the application of the proposed CAPEX model to the

**Table 3**
CAPEX breakdown: unitary costs. Adapted from [60].

| Definition | Value | Units |
|---|---|---|
| Cost of occupation of the farm (taxes) | 2.00 | €/m$^2$ |
| Cost of carbon steel manufactured for the structure of the nacelle | 8.00 | €/kg |
| Cost of manufactured carbon steel for PTO frame | 4.00 | €/kg |
| Cost of manufactured fiberglass for the fairing | 10.00 | €/kg |
| Cost of thrust bearing | 40,000.00 | €/MW |
| Cost of brake system | 2000.000 | €/MW |
| Cost of electrical generator | 180,000.00 | €/MW |
| Cost of gearbox | 35,000.00 | €/MW |
| Cost of high-speed shaft | 3000.00 | €/MW |
| Cost of yaw system | 12.00 | €/kg |
| Cost of cooling system | 15,000.00 | €/MW |
| Cost of pressure oil system | 15,000.00 | €/MW |
| Cost of condition monitoring system | 110,000.00 | €/MW |
| Cost of protection and connection switches | 12.00 | €/kg |
| Cost of control system | 12.00 | €/kg |
| Cost of bilge system | 12.00 | €/kg |
| Cost of compressed air system | 12.00 | €/kg |
| Cost of circuit board | 12.00 | €/kg |
| Cost of added elements | 3.00 | €/kg |
| Cost of blades | 40.00 | €/m |
| Cost of pitch system | 500.00 | €/m |
| Cost of core of the rotor | 1000.00 | €/m |
| Cost of low-speed shaft | 500.00 | €/m |
| Cost of base support of the HEC structure | 3.00 | €/kg |
| Cost of transition structure of the HEC | 3.00 | €/kg |
| Cost of vertical column of the HEC | 3.00 | €/kg |
| Cost of elaborated concrete of the ballast | 0.20 | €/kg |
| Cost of special concrete bags | 0.30 | €/kg |
| Cost of mooring system (catenary anchor leg mooring) composed by three stud–link chain lines | 40.00 | €/m |
| Cost of concrete monopile foundation up to 30 m water depth | 15,000.00 | €/m |
| Cost of protection switch | 25,000.00 | €/MW |
| Cost of submarine connector | 25.00 | €/kg |
| Cost of submarine connector installed in the base of the HEC | 12.00 | €/kg |
| Cost of internal wiring | 12.00 | €/kg |
| Cost of connection box | 12.00 | €/kg |
| Cost of umbilical cables | 250.00 | €/m |
| Cost of rectifiers | 100,000.00 | €/MW |
| Cost of inverters | 100,000.00 | €/MW |
| Cost of electrical boxes | 20,000.00 | €/MW |
| Cost of transformers | 40,000.00 | €/MW |
| Cost of transformation platform | 3.00 | €/kg |
| Cost of submarine exportation cables | 500.00 | €/m |
| Cost of ground exportation cables | 150.00 | €/m |

Tarbert Area are presented in Table 4. As can be observed, $CAPEX_2$ represents the lion's share of the total capital investment, followed by $CAPEX_1$ (about ten times less) and $CAPEX_3$ (about forty times less). However, their relative importance for the different HEC-site combinations differs widely; in effect, as the surface considered (and therefore the number of HECs) increases, the value of $CAPEX_2$ significantly increases, whereas this increase in the case of $CAPEX_1$ is much more contained. This means that in the case of areas of reduced surface (e.g., about 5 hm$^2$), the contribution of $CAPEX_1$ to the total CAPEX could represent 50% of $CAPEX_2$.

## 6. OPEX model

### 6.1. Fundamentals of OPEX estimation

OPEX represent the expenditures incurred during the operation, in this case, of a hydrokinetic farm. They usually include all the expenses related with the fixed costs of exploitation and both scheduled and unscheduled O&M, such as insurances, taxes, salaries, facilities, etc [25]. In consequence, OPEX are highly influenced by the performance of the plant and the O&M strategy defined for each type of installation. As a general rule, they constitute an important driver of the cost structure of a hydrokinetic farm, reaching average figures greater than 30% of the total expenses [45]; however, they may widely vary amongst hydrokinetic farms depending on their specific characteristics [25]. Resulting from their importance on the cost structure of a hydrokinetic farm, it is necessary to estimate OPEX as realistically as possible, analysing in detail the actual limitations of the state of the art. To this end, an ad hoc OPEX model is developed (Section 6.2) by considering: (i) reliability HEC data (Section 3), (ii) high-resolution hydrodynamic numerical modelling (Section 4), and (iii) several O&M procedures. Finally, this model is applied to estimate the OPEX of the different HEC-site combinations defined for the Tarbert Area (Section 6.3).

In spite of their important weight on the cost structure of hydrokinetic farms, the assessment of OPEX is subject to a large number of uncertainties, which results from the lack of knowledge caused by the reduced number of real projects. In order to avoid these difficulties, OPEX estimations usually resort to considering either specific cost items or the total cost as a function of the installed power [46,71] or as percentage of CAPEX [25,72]. Recent works proposed more complex models for specific maintenance items, including O&M schemes based on metocean data [47,73,74]; however, high-resolution site-specific numerical modelling required for accurate OPEX estimations is not usually considered [25]. Moreover, previous studies are focused on specific designs of HECs and only take into account a specific O&M strategy [25,60,63–65]. These weaknesses are considered as a starting point for the development of an ad hoc OPEX model, which is detailed in the subsequent section (Section 6.2).

In this regard, prior to the development of an OPEX model, it is necessary to define an appropriate breakdown whose categories would allow a developer to consider all the aforementioned aspects. In the present work, as in the case of CAPEX, a breakdown of OPEX composed of three different categories is considered [25,60,63,75]: (i) insurances and fixed costs ($OPEX_1$), which represent one of the most expensive maintenance costs in renewables [76]; (ii) scheduled or preventive maintenance ($OPEX_2$), covering calendar- or condition-based supervising and reconditioning works; and (iii) unscheduled or corrective maintenance ($OPEX_3$), which stands for unplanned repairing operations. The evaluation of these cost categories in the proposed model is explained in detail in Section 6.2.

**Table 4**
CAPEX results (M€) for the different HEC-site combinations considered.

| Cost item | F-HEC—A | F-HEC—B | F-HEC—C | F-HEC—D | F-HEC—E | F-HEC—IHE | BF-HEC—E |
|---|---|---|---|---|---|---|---|
| $CAPEX_1$ | **5.72** | **5.92** | **6.48** | **7.53** | **9.73** | **11.38** | **5.75** |
| $CAPEX_2$ | **12.91** | **22.64** | **48.02** | **100.71** | **213.71** | **295.90** | **61.65** |
| HECs | 6.50 | 13.25 | 30.21 | 64.74 | 136.72 | 190.25 | 24.11 |
| Foundations | n.a. | n.a. | n.a. | n.a. | n.a. | n.a. | 13.54 |
| Moorings | 0.70 | 1.55 | 4.23 | 10.87 | 27.43 | 37.64 | n.a. |
| Cabling | 5.71 | 7.84 | 13.58 | 25.10 | 49.56 | 68.01 | 24.00 |
| $CAPEX_3$ | **0.15** | **0.33** | **0.99** | **1.77** | **3.53** | **5.64** | **1.40** |
| Power system | 0.02 | 0.04 | 0.13 | 0.23 | 0.47 | 0.75 | 0.19 |
| Cabling | 0.04 | 0.08 | 0.26 | 0.46 | 0.92 | 1.46 | 0.36 |
| HECs | 0.09 | 0.21 | 0.60 | 1.08 | 2.14 | 3.42 | 0.85 |
| CAPEX | **18.78** | **28.89** | **55.49** | **110.01** | **226.97** | **312.91** | **68.80** |

**Table 5**
Hydrodynamic thresholds for the operation and maintenance works using OSV and CTV vessels.

| Weather criteria | OSV O&M | CTV O&M |
|---|---|---|
| Significant wave height, $H_s$ (m). Safety and (max.) values | 1.50 (2.00) | 1.20 (1.50) |
| Tidal currents velocity, $V_{tc}$ (m/s) | 1.00 | 1.00 |
| Wind velocity at 10 m height, $U_{10}$ (m/s) | 10.00 | 10.00 |

### 6.2. Definition of OPEX model

The approach proposed in this work addresses the abovementioned limitations of current OPEX models by considering: (i) high-resolution site-specific numerical modelling; and (ii) different O&M procedures, as a result of analysing HECs representative of various taxonomies (Section 3). The first aspect is of paramount importance to provide the required accuracy for the definition of weather windows suitable for the O&M works; the second one has an important influence resulting from the differences in the maintenance protocol of floating and bottom-fixed technologies (e.g., number of technicians required, type of vessel, duration of works, etc.). Bearing this in mind, the evaluation of $OPEX_1$, $OPEX_2$ and $OPEX_3$ is developed as follows.

The accurate estimation of $OPEX_1$ represents a complex task given the low number of real projects developed; thus, reference values should be provided by developers and stakeholders, in particular from the offshore sector [76]. In this regard, as in the case of the abovementioned simplified estimations of OPEX, it is usual to estimate this term as a function of the installed power or as a percentage of the CAPEX. The approach followed in this work is the second, with $OPEX_1$ computed as a 1.5% of CAPEX, which has shown to provide accurate results [25,72].

Regarding $OPEX_2$, it encompasses very heterogeneous maintenance works, covering from cleaning and inspection activities to the replacement of minor components belonging to different systems of the hydrokinetic farm [75]. Thus, this term is the result of several cost items incurred during these works, whose amounts could be highly diverse (e.g., material, staff, transport, etc.). In this respect, the accurate definition of weather windows suitable for conducting maintenance works has a key role in driving the expenses included within the $OPEX_2$ term [60,63], and therefore lead to an optimization of resources and costs [75].

The computation of these weather windows requires the definition of specific hydrodynamic conditions, usually in form of threshold values, considering the different weather parameters that could influence the maintenance works and their implication for the security of the infrastructure and workers involved. In this regard there exist different types of vessels to conduct maintenance operations, which can be divided in two large categories [77]: (i) Crew Transport Vessel (CTV) for offshore reparations, and (ii) an Offshore Supply Vessel (OSV), usually equipped with a Remoted Operated Vehicle (ROV), in the case of onshore works. OSV operation requires specific wave, wind and current conditions, whereas CTV operation is only limited in terms of wave height [77]; however, given that specific specialized workers (e.g., divers or

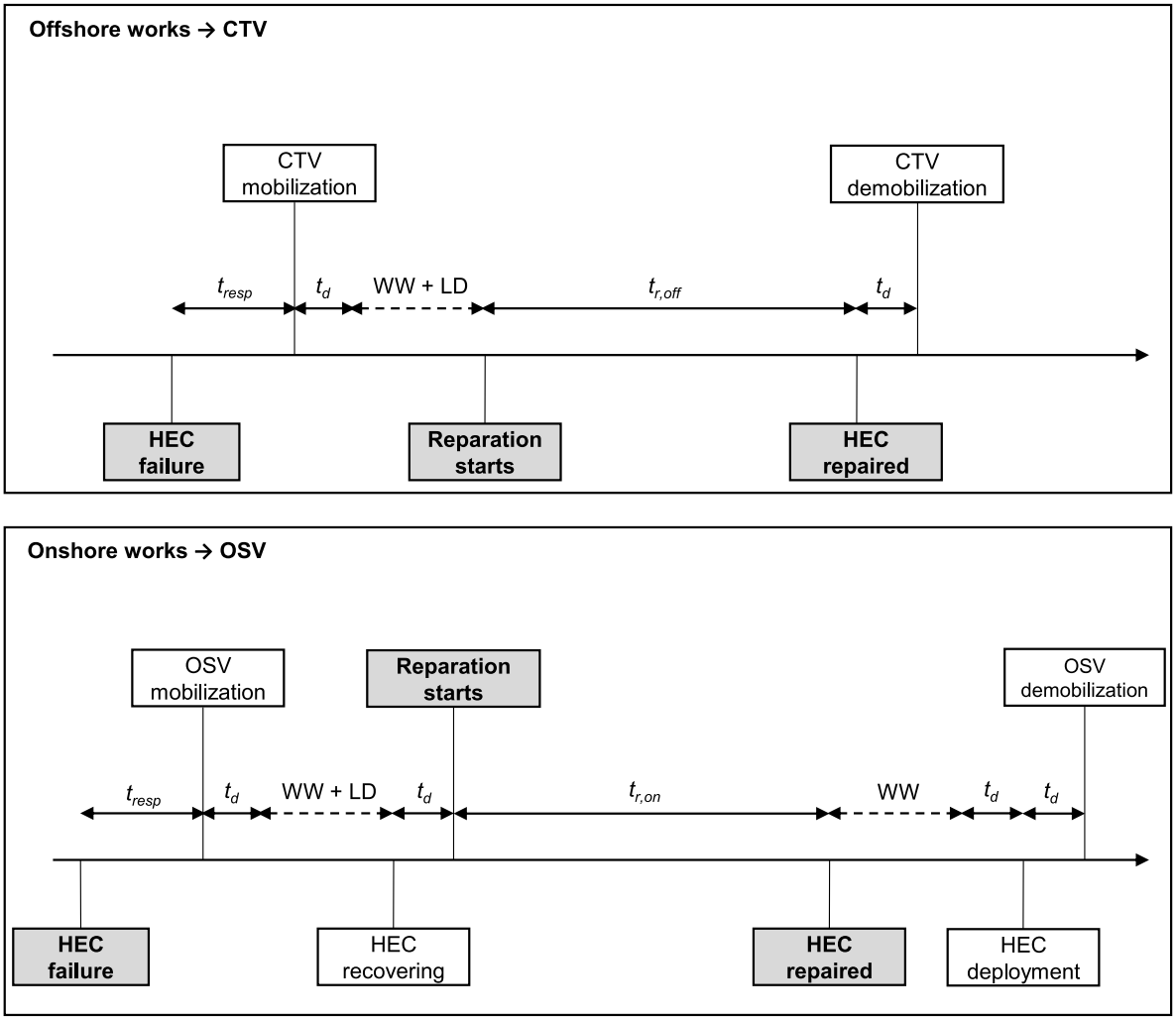


**Fig. 8.** Sketch of the operational protocol for offshore (above) and onshore (below) unplanned reparations ($OPEX_3$).

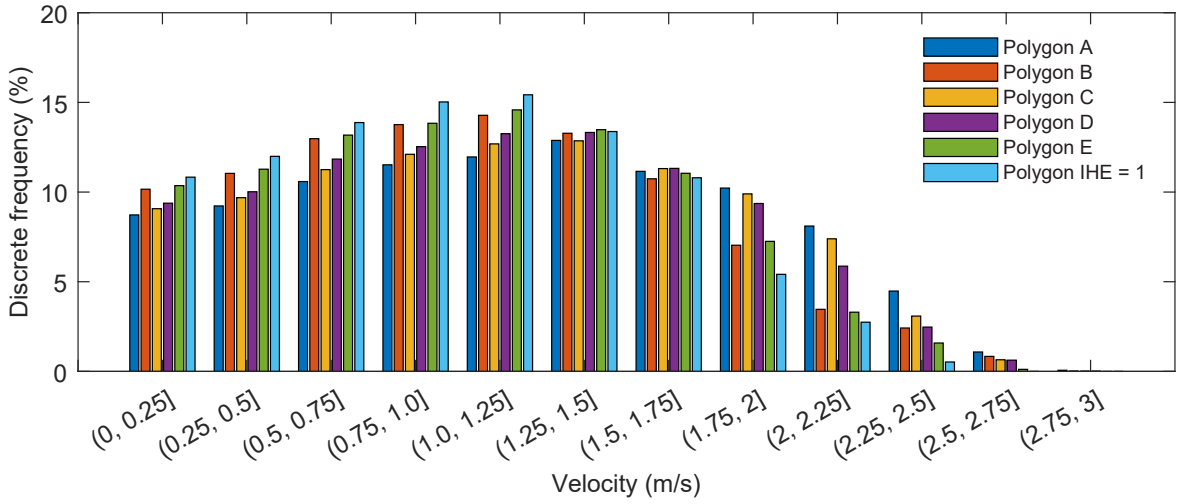


**Fig. 9.** Discrete frequency (non-exceedance) of velocity intervals (0.25 m/s wide) for the polygons considered.

submarine welders) also require specific conditions, CTV operation is also limited by wind and current conditions [25]. Table 5 summarizes the different hydrodynamic thresholds, which are defined by considering not only the limit conditions for the operation of the vessels but also, as abovementioned, the security of workers, which results in considerably restrictive conditions, especially in terms of current velocity [25].

In the case of areas of interest for HEC operation sheltered from wave action, it can be assumed that the only limiting condition is the magnitude of the currents, and therefore, weather windows should be computed based on high-resolution hydrodynamic numerical modelling (Shallow Water models) leading to the accurate computation of its discrete and cumulative annual velocity frequencies. This computation should be conducted by considering the time during which the aforementioned threshold is not exceeded and, therefore, the hydrodynamic conditions are suitable for maintenance operations. It is important to note that the need for considering waves and winds should be analysed for each case study.

In this work $OPEX_2$ is computed based on reference values for the different parameters involved in its computation [60] which are adapted to the site-specific conditions of the different HEC-site combinations (Section 3) in terms of weather windows appropriate for O&M works (Table 5).

In the case of $OPEX_3$, the definition of an appropriate operational protocol is a key aspect for conducting unplanned repairing operations, allowing the optimization of material and human resources [75]. In this context, the repairing strategy needs to be adapted according to the vertical configuration of the hydrokinetic farm, distinguishing between bottom-fixed and floating converters [77]. These vertical configuration influences not only the different resources involved in the repairing procedure and its location (i.e., onshore or offshore) but also the accessibility to the different components of HECs.

According to Ref. [77], these protocols are defined as follows: in the case of bottom-fixed HECs, their unplanned maintenance is, in any case, conducted at onshore facilities; on the contrary, the unplanned maintenance of floating HECs can be carried out either onshore or offshore, depending on the duration of the works, $t_r$. For trivial works ($t_r \leq 1$ h), the reparations can be conducted offshore. Minor reparations (1 h $< t_r \leq$ 24 h) are usually prescribed offshore if the components of the HEC are easily accessible, and at onshore facilities in the opposite case. Finally, major reparations ($t_r >$ 24 h), are always conducted onshore. This categorization has an effect on the type of vessel required for conducting the repairing works (CTV and OSV for offshore and onshore maintenance, respectively), as in the case of OPEX2 computation (see above). In Fig. 8 the operational protocol for both offshore and onshore unplanned reparations is presented in the terms of the following timing nomenclature [77]: $t_{resp}$ is the response time, which represents the time necessary to detect a failure and mobilize the human and technical resources required; $t_d$ stands for the displacement time, considering the distance between the base port and the hydrokinetic farm; WW represents the time increment incurred as a consequence of weather windows; LD stands for time increments resulting from logistic delays; and finally, $t_{r,off}$ and $t_{r,on}$ are representative timings of repairing operations for offshore and onshore works, respectively. Further information regarding the cost of the resources involved in both protocols can be found in Ref. [25]. As in the case of $OPEX_2$, an accurate computation of $OPEX_3$ should be based on the definition of the required weather windows as previously defined (Table 5).

Based on the aspects previously remarked, the computation of the $OPEX_3$ term can be summarized in the following steps: (i) definition of the operational protocol as a function of the vertical configuration of the hydrokinetic farm, (ii) computation of the costs incurred as a result of each repairing operation depending on the timing and resources involved, (iii) evaluation of the impact of weather windows and delays on the cost of each operation, (iv) computation of $OPEX_3$ term by considering the reliability of the devices (required annual number of interventions), and integrating the results of steps (i), (ii) and (iii).

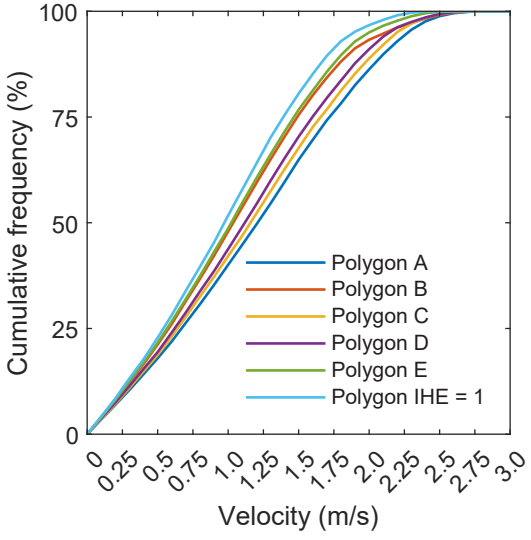


**Fig. 10.** Cumulative frequency (non-exceedance) of flow velocity for the polygons considered.

**Table 6**
Timing (average values) of the different activities conducted during repairing or unscheduled maintenance works ($OPEX_3$) for offshore and onshore operations.

| Variable | Duration |
|---|---|
| $t_c$ | 1.00 h |
| $t_d$ | 0.50 h |
| WW | Site-specific |
| LD | 30% (time increase) |
| $t_{r,off}$ | 4.00 h |
| $t_{r,on}$ | 32.00 h |

### 6.3. Application of OPEX model

For the application of the model, in the first place the annual discrete and cumulative velocity frequencies (non-exceedance) are obtained from the high-resolution shallow water model, and presented in Figs. 9 and 10, respectively.

The time available for O&M for the different areas is similar, despite their differences in total surface, with about 40.1%, 47.9%, 42.21%, 43.8%, 48.9% and 51.7% for polygons A, B, C, D, E, and IHE = 1, respectively (Fig. 10). It can be observed that the smaller the polygons, the higher IHE tend to have large resource, and therefore large current magnitude which reduce the available time for O&M. However, given that IHE index also considers the costs (in a somewhat simplistic way), this does not apply to all cases, as it can be observed in the case of polygon B which presents greater O&M windows than larger polygons such as C and D.

Based on these figures, the proposed OPEX model is applied to the Tarbert Area by considering the Tarbert facilities as base port (Fig. 1) in order to compute the timing of the works associated to the operational protocols for unplanned reparations shown in Fig. 8 (Table 6) [25]. The results of the application of the OPEX model are provided in Table 7.

As can be observed, $OPEX_1$ and $OPEX_2$ represent the lion's share of the operational expenditures, being about one order magnitude larger than $OPEX_3$. Overall $OPEX_2$ is larger than $OPEX_1$ (more than double considering all HEC-site combinations); however, their relative importance is highly dependent on the total surface and the resulting number of HECs considered, being $OPEX_1$ greater than $OPEX_2$ in the case of polygon A.

## 7. CEA parameters computation

The results obtained for AEP, OPEX and CAPEX can be straightforwardly used to compute the viability of the proposed HEC-site combination through CEA parameters. As previously mentioned, in this application CEA is developed in terms of Levelized Cost of Energy (LCOE), which is usually computed as follows [45]:

$$LCOE = \frac{CAPEX + \sum_{t=1}^{T} \frac{OPEX}{(1+k)^t}}{\sum_{t=1}^{T} \frac{AEP}{(1+k)^t}}, \tag{3}$$

where $k$ represents the discount rate and $T$ is the lifetime of the project. According to Ref. [24], values of 10% and 20 years are established for $k$ and $T$, respectively. In addition, it is important to note that the discount rate is not applied to CAPEX insofar as this term corresponds with initial investments which are not constant along the lifetime of the project. The interpretation of the LCOE is straightforward: the lower the value of the LCOE, the better the HEC-site combination for hydrokinetic energy exploitation.

In Fig. 11, LCOE results for the different HEC-site combinations are presented. It can be observed that LCOE values reduce as the polygons occupy progressively a larger area as a result of the effects of the economies of scale, and up to a point where they attain their largest influence (i.e., reach a constant peak value), thereby providing the largest cost reduction. In the case of F-HEC: polygons A with 0.314 €/kWh, B with 0.310 €/kWh, C with 0.196 €/kWh, D with 0.200 €/kWh, E with 0.247 €/kWh and IHE = 1 with 0.287 €/kWh. In the case of BF-HEC, its LCOE in polygon E is 0.260 €/kWh.

Thus, in spite of the smallest polygon (polygon A) being that with the largest $C_f$ and IHE index, the effects of the economies of scale lead to a polygon with larger available area and less available resource (power), polygon C, to be that providing the best cost-effective figures, which are attained by F-HEC.

The results of LCOE obtained are compared with those obtained by applying previous state-of-the-art procedures used in tidal energy projects. To this end, simplistic procedures for easily assessing the viability of projects at their initial steps (e.g. Refs. [24,78,79]), along with complex procedures providing more accurate results (e.g. Refs. [45,46,61]) are considered. The comparison is conducted for the selected combinations: F-HEC operating in polygon C and BF-HEC operating in

**Table 7**
Annual OPEX results (M€) for the HEC-site combinations considered.

| Cost item | F-HEC—A | F-HEC—B | F-HEC—C | F-HEC—D | F-HEC—E | F-HEC—IHE | BF-HEC—E |
|---|---|---|---|---|---|---|---|
| $OPEX_1$ | 0.28 | 0.43 | 0.83 | 1.65 | 3.40 | 4.69 | 1.03 |
| $OPEX_2$ | 0.26 | 0.56 | 1.47 | 3.12 | 6.38 | 8.70 | 2.53 |
| $OPEX_3$ | 0.04 | 0.04 | 0.04 | 0.04 | 0.04 | 0.04 | 0.1 |
| OPEX | **0.58** | **1.03** | **2.34** | **4.81** | **9.82** | **13.43** | **3.66** |

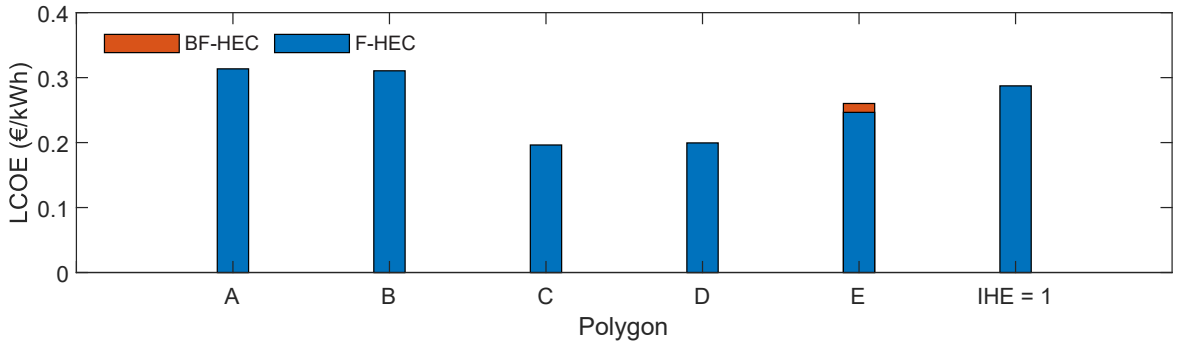


**Fig. 11.** LCOE of the HEC-site combinations considered.

**Table 8**
Comparison of the results of LCOE according to the proposed methodology ($LCOE_{IHE}$) and other state-of-the-art procedures ([24,78,79] and [45,45,61]).

| HEC-site combination | $LCOE_{IHE}$ (€/kWh) | LCOE [24,78,79] (€/kWh) | LCOE [45,45,61] (€/kWh) |
|---|---|---|---|
| F-HEC—C | 0.196 | 0.397 | 0.280 |
| BF-HEC—E | 0.260 | 0.688 | 0.560 |

polygon E. For the application of these methodologies CAPEX and OPEX terms are computed, whereas AEP is determined according to section 4. LCOE results are provided in Table 8.

As it can be observed, the implementation of more simplistic theories, in particular [24,78,79] leads to significant deviations in LCOE figures with respect to the proposed methodology in the present study, of about 103% and 165% for F-HEC in polygon C and BF-HEC in polygon E, respectively. The application of more detailed methodologies [45,46,61] provides more accurate results, with deviations of about 43% and 115%, for F-HEC in polygon C and BF-HEC in polygon E, respectively.

The deviations in the results obtained are primarily due to how OPEX is computed following the different procedures, which correspond to either predetermined values according to general farm characteristics, in the case of simple procedures, or are function of the installed power of the farm, in the case of more complex methodologies. In this way, the current available procedures do not consider cost reductions with increasing farm size, and therefore they usually overestimate OPEX values for large farm projects, as it is the case of the present study.

## 8. Conclusions

Cost-effective analyses (CEA) of proposed hydrokinetic farms are often based on highly simplified energy performance parameters and cost structure, which may lead to suboptimal planning decisions. In connection with the development of CEA is the delimitation of the areas of analysis, usually defined by merely considering the available energy resource and, in some occasions, certain geomorphological parameters, such as the total water depth. These simplified approaches could be adequate in the initial stages of the design of a hydrokinetic farm; however, further and more detailed information is required for the accurate definition of the most appropriate configuration. The current methodologies applied to tidal energy projects only approximate the correct values of the CEA parameters, as a result of their inability to consider specific aspects of the cost analysis, in particular O&M costs, and their disregard of the potential effects of economies of scale, which are related to the characteristics of the study areas (total surface, distance to existing ports, hydrodynamics, etc.).

In this work, a novel approach for accurately computing CEA parameters of hydrokinetic energy projects is developed, leading to the selection of the most appropriate HEC-site combination within a coastal area, and improving previous procedures. The proposed methodology is subsequently applied to the Shannon Estuary (W Ireland) and the results computed in terms of Levelized Cost of Energy (LCOE).

The proposed approach consists of five steps. First, a HEC-site selection model is developed by means of the IHE index and spatial analysis algorithms, leading to the definition of various HEC-site combinations which allow the consideration of economies of scale by retaining different areas for analysis based on specific criteria. Then, the application of an energy production model leads to the computation of the Annual Energy Production (AEP) for the different HEC-site combinations selected, for which high-resolution numerical modelling and specific algorithms are considered. With respect to the cost structure, a Capital Expenditures (CAPEX) model and an Operational Expenditures (OPEX) model are developed. The CAPEX model is based on the detailed breakdown in unitary costs and an ad hoc algorithm for assessing the effects of the economies of scale of the different HEC-site combinations retained. The OPEX model considers HEC-specific O&M procedures, including the analysis of the necessary human and material resources, along with the definition of specific O&M weather windows. Finally, the previous results are integrated to provide reliable CEA parameters for the different HEC-site combinations, leading to the selection of the best alternative.

This procedure is illustrated for the Shannon Estuary and, in particular, the Tarbert Area. The CEA parameters are obtained in terms of Levelized Cost of Energy (LCOE). It is found that the area with the largest $C_f$ and IHE index is not that with the best CEA parameters; instead, the economies of scale lead to a larger area with less available resource providing the best cost-effective figures. As a result, the HEC-site combination providing best cost-effective figures is F-HEC at polygon C with 0.196 €/kWh. The results of LCOE obtained are compared with those obtained by applying state-of-the art procedures used in tidal energy projects. Significant variations in LCOE results as obtained from the different methodologies considered are observed ranging from about 40% to 165%, which results from the overly simplistic OPEX computations leading to a significant overestimation of cost in the case of large farms. In sum, the proposed approach addresses the major difficulties and uncertainties when computing the main aspects affecting the CEA of hydrokinetic energy farms, avoiding simplistic assumptions, and overall improving on the current procedures. The procedure was illustrated through a case study in the Shannon Estuary, but it could be applied to any other coastal area with potential for hydrokinetic energy exploitation.

## CRediT authorship contribution statement

**D.M. Fouz:** Conceptualization, Methodology, Investigation, Formal analysis, Visualization, Writing – original draft. **R. Carballo:** Conceptualization, Methodology, Writing – review & editing, Supervision, Project administration, Funding acquisition. **I. López:** Methodology, Formal analysis, Writing – review & editing, Supervision. **X.P. González:** Methodology, Formal analysis, Visualization, Supervision. **G. Iglesias:** Conceptualization, Methodology, Writing – review & editing, Supervision.

## Declaration of competing interest

The authors declare that they have no known competing financial interests or personal relationships that could have appeared to influence the work reported in this paper.

## Data availability

The authors are unable or have chosen not to specify which data has been used.

## Acknowledgements

This work was supported by the PORTOS project, which is co-financed by the Interreg Atlantic Area Programme, through the European Regional Development Fund [grant number EAPA_784/2018] and 'Axudas para a consolidación e estruturación de unidades de investigación competitivas nas universidades do Sistema Universitario Galego (2020–22)' with reference number ED341B 2020/25.

During this work, D.M. Fouz was supported by a predoctoral grant of the 'Convocatoria de contratos predoutorais do Campus de Especialización Campus Terra' with reference number 8042-272B-64100.

## References

[1] Robbins JR, Buchet PJ, Miller DL, Evans PGH, Waggitt J, Ford AT, et al. Shipping in the north-east Atlantic: identifying spatial and temporal patterns of change. Mar Pollut Bull 2022;179:113681.

[2] Anticamara JA, Watson R, Gelchu A, Pauly D. Global fishing effort (1950–2010): trends, gaps, and implications. Fish Res 2011;107:131–6.
[3] Baxter T, Coombes M, Viles H. Identifying priorities for the joint conservation of maritime built heritage and marine biodiversity: an assessment of shoreline engineering on the Isles of Scilly, UK, using historical datasets. Ocean Coast Manag 2022;227:106288.
[4] Filho LM, Roebeling P, Villasante S, Bastos MI. Ecosystem services values and changes across the Atlantic coastal zone: considerations and implications. Mar Pol 2022;145:105265.
[5] Ramos V, Giannini G, Calheiros-Cabral T, Rosa-Santos P, Taveira-Pinto F. Legal framework of marine renewable energy: a review for the Atlantic region of Europe. Renew Sustain Energy Rev 2021;137:110608.
[6] Claus R, López M. Key issues in the design of floating photovoltaic structures for the marine environment. Renew Sustain Energy Rev 2022;164:112502.
[7] Pérez-Collazo C, Greaves D, Iglesias G. A review of combined wave and offshore wind energy. Renew Sustain Energy Rev 2015;42:141–53.
[8] Todeschini G, Coles D, Lewis M, Popov I, Angeloudis A, Fairley I, et al. Medium-term variability of the UK's combined tidal energy resource for a net-zero carbon grid. Energy 2022;238:121990.
[9] Almoghayer MA, Woolf DK, Kerr S, Davies G. Integration of tidal energy into an island energy system – a case study of Orkney islands. Energy 2022;242:122547.
[10] Li J, Pan S, Chen Y, Yao Y, Xu C. Assessment of combined wind and wave energy in the tropical cyclone affected region:An application in China seas. Energy 2022;260:125020.
[11] Neill SP, Angeloudis A, Robins PE, Walkington I, Ward SL, Masters I, et al. Tidal range energy resource and optimization – past perspectives and future challenges. Renew Energy 2018;127:763–78.
[12] Carballo R, Sánchez M, Ramos V, Taveira-Pinto F, Iglesias G. A high resolution geospatial database for a wave energy exploitation. Energy 2014;68:572–83.
[13] Pugh DT. Tides, surges, and mean sea-level/a handbook for engineers and scientists. John Wiley & Sons Inc; 1996.
[14] Dyer KE. Estuaries: a physical introduction. New York: John Wiley; 1997.
[15] Saini G, Saini RP. A review on technology, configurations, and performance of cross-flow hydrokinetic turbines. Int J Energy Res 2019;43:6639–79.
[16] Seo J, Yi J, Park J, Lee K. Review of tidal characteristics of Uldolmok Strait and optimal design of blade shape for horizontal axis tidal current turbines. Renew Sustain Energy Rev 2019;113:109273.
[17] Segura E, Morales R, Somolinos JA, López A. Techno-economic challenges of tidal energy conversion systems: current status and trends. Renew Sustain Energy Rev 2017;77:536–50.
[18] Kim ES, Bernitsas MM. Performance prediction of horizontal hydrokinetic energy converter using multiple-cylinder synergy in flow induced motion. Appl Energy 2016;170:92–100.
[19] Fouz DM, Carballo R, Ramos V, Iglesias G. Hydrokinetic energy exploitation under combined river and tidal flow. Renew Energy 2019;143:558–68.
[20] Iglesias I, Bio A, Bastos L, Avilez-Valente P. Estuarine hydrodynamic patterns and hydrokinetic energy production: the Douro estuary case study. Energy 2021;222:119972.
[21] Si Y, Liu X, Wang T, Feng B, Qian P, Ma Y, et al. State-of-the-art review and future trends of development of tidal current energy converters in China. Renew Sustain Energy Rev 2022;167:112720.
[22] Bahaj A, Blunden L, Anwar A. Tidal-current energy device development and evaluation protocol. University of Southampton; 2008. Southhampton, Tech.Rep.
[23] Robertson B, Bekker J, Buckham B. Renewable integration for remote communities: comparative allowable cost analyses for hydro, solar and wave energy. Appl Energy 2020;264:114677.
[24] Vazquez A, Iglesias G. LCOE (levelised cost of energy) mapping: a new geospatial tool for tidal stream energy. Energy 2015;91:192–201.
[25] López A, Morán JL, Núñez LR, Somolinos JA. Study of a cost model of tidal energy farms in early design phases with parametrization and numerical values. Application to a second-generation device. Renew Sustain Energy Rev 2020;117:109497.
[26] Rodrigues N, Pintassilgo P, Calhau F, González-Gorbeña E, Pacheco A. Cost-benefit analysis of tidal energy production in a coastal lagoon: the case of Ria Formosa – Portugal. Energy 2021;229:120812.
[27] Radfar S, Panahi R, Javaherchi T, Filom S, Mazyaki AR. A comprehensive insight into tidal stream energy farms in Iran. Renew Sustain Energy Rev 2017;79:323–38.
[28] de Andres A, Medina-Lopez E, Crooks D, Roberts O, Jeffrey H. On the reversed LCOE calculation: design constraints for wave energy commercialization. International Journal of Marine Energy 2017;18:88–108.
[29] Iglesias G, Sánchez M, Carballo R, Fernández H. The TSE index – a new tool for selecting tidal stream sites in depth-limited regions. Renew Energy 2012;48:350–7.
[30] Fouz DM, Carballo R, López I, Iglesias G. Tidal stream energy potential in the Shannon Estuary. Renew Energy 2022;185:61–74.
[31] Fouz DM, Carballo R, López I, Iglesias G. A holistic methodology for hydrokinetic energy site selection. Appl Energy 2022;317:119155.
[32] Castro-Santos L, Filgueira-Vizoso A, Lamas-Galdo I, Carral-Couce L. Methodology to calculate the installation costs of offshore wind farms located in deep waters. J Clean Prod 2018;170:1124–35.
[33] Dismukes DE, Upton GB. Economies of scale, learning effects and offshore wind development costs. Renew Energy 2015;83:61–6.
[34] Robins PE, Neill SP, Lewis MJ, Ward SL. Characterising the spatial and temporal variability of the tidal-stream energy resource over the northwest European shelf seas. Appl Energy 2015;147:510–22.
[35] Coles D, Angeloudis A, Greaves D, Hastie G, Lewis M, Mackie L, et al. A review of the UK and British Channel Islands practical tidal stream energy resource. Proc Roy Soc Lond 2021;477:20210469.
[36] Manchester S, Barzegar B, Swan L, Groulx D. Energy storage requirements for in-stream tidal generation on a limited capacity electricity grid. Energy 2013;61:283–90.
[37] Barbour E, I GB. Energy storage in association with tidal current generation systems. Proc Inst Mech Eng: J Power Energy 2011;225:443–55.
[38] Coles D, Angeloudis A, Goss Z, Miles J. Tidal stream vs. Wind energy: the value of cyclic power when combined with short-term storage in hybrid systems. Energies 2021;14.
[39] Clarke JA, Connor G, Grant AD, Johnstone CM. Regulating the output characteristics of tidal current power stations to facilitate better base load matching over the lunar cycle. Renew Energy 2006;31:173–80.
[40] Bryden IG, Macfarlane DM. The utilisation of short term energy storage with tidal current generation systems. Energy 2000;25:893–907.
[41] SIFP Steering Group. Strategic Integrated Framework Plan (SIFP) for the Shannon Estuary - an inter-jurisdictional land and marine based framework to guide the future developments and management of the Shannon Estuary. 2013.
[42] O'Rourke F, Boyle F, Reynolds A. Ireland's tidal energy resource; an assessment of a site in the Bulls Mouth and the Shannon Estuary using measured data. Energy Convers Manag 2014;87:726–34.
[43] Arean N, Carballo R, Iglesias G. An integrated approach for the installation of a wave farm. Energy 2017;138:910–9.
[44] Álvarez M, Carballo R, Ramos V, Iglesias G. An integrated approach for the planning of dredging operations in estuaries. Ocean Eng 2017;140:73–83.
[45] Vazquez A, Iglesias G. Capital costs in tidal stream energy projects – a spatial approach. Energy 2016;107:215–26.
[46] Vazquez A, Iglesias G. A holistic method for selecting tidal stream energy hotspots under technical, economic and functional constraints. Energy Convers Manag 2016;117:420–30.
[47] T MD, D Z, P JT. Tidal stream device reliability comparison models. Proc Inst Mech Eng O J Risk Reliab 2012;226:6–17.
[48] Sánchez M, Carballo R, Ramos V, Iglesias G. Energy production from tidal currents in an estuary: a comparative study of floating and bottom-fixed turbines. Energy 2014;77:802–11.
[49] Díaz H, Rodrigues JM, Guedes Soares C. Preliminary assessment of a tidal test site on the Minho estuary. Renew Energy 2020;158:642–55.
[50] Han J, Jung J, Hwang JH. Optimal configuration of a tidal current turbine farm in a shallow channel. Ocean Eng 2021;220:108395.
[51] Radfar S, Panahi R, Majidi Nezhad M, Neshat M. A numerical methodology to predict the maximum power output of tidal stream arrays. Sustainability 2022;14.
[52] Funke SW, Kramer SC, Piggott MD. Design optimisation and resource assessment for tidal-stream renewable energy farms using a new continuous turbine approach. Renew Energy 2016;99:1046–61.
[53] Ren Z, Wang Y, Li H, Liu X, Wen Y, Li W. A coordinated planning method for micrositing of tidal current turbines and collector system optimization in tidal current farms. IEEE Trans Power Syst 2019;34:292–302.
[54] Fakhri E, Thiébot J, Gualous H, Machmoum M, Bourguet S. Overall tidal farm optimal design–application to the alderney race and the fromveur strait (France). Appl Ocean Res 2021;106:102444.
[55] Iglesias G, Carballo R. Can the seasonality of a small river affect a large tide-dominated estuary? The case of the Ria de Viveiro, Spain. J Coast Res 2011;27:1170–82.
[56] Ramos V, Carballo R, Álvarez M, Sánchez M, Iglesias G. A port towards energy self-sufficiency using tidal stream power. Energy 2014;71:432–44.
[57] Pacheco A, Ferreira Ó, Carballo R, Iglesias G. Evaluation of the production of tidal stream energy in an inlet channel by coupling field data and numerical modelling. Energy 2014;71:104–17.
[58] Fouz DM, Carballo R, López I, Ramos V, Iglesias G. Hydrokinetic energy production in shallow estuaries: miño estuary, nw Spain. Proceedings of the European Wave and Tidal Energy Conference 2021. 1995-1.
[59] Ramos V, Iglesias G. Performance assessment of tidal stream turbines: a parametric approach. Energy Convers Manag 2013;69:49–57.
[60] Segura E, Morales R, Somolinos JA. Cost assessment methodology and economic viability of tidal energy projects. Energies 2017;10.
[61] Allan G, Gilmartin M, McGregor P, Swales K. Levelised costs of wave and tidal energy in the UK: cost competitiveness and the importance of "banded" renewables obligation certificates. Energy Pol 2011;39:23–39.
[62] Payne GS, Stallard T, Martinez R. Design and manufacture of a bed supported tidal turbine model for blade and shaft load measurement in turbulent flow and waves. Renew Energy 2017;107:312–26.
[63] Segura E, Morales R, Somolinos JA. Economic-financial modeling for marine current harnessing projects. Energy 2018;158:859–80.
[64] Segura E, Morales R, Somolinos JA. Increasing the competitiveness of tidal systems by means of the improvement of installation and maintenance maneuvers in first generation tidal energy converters—an economic argumentation. Energies 2019;12.
[65] Segura E, Morales R, Somolinos JA. Influence of automated maneuvers on the economic feasibility of tidal energy farms. Sustainability 2019;11.
[66] Carballo R, Iglesias G, Castro A. Numerical model evaluation of tidal stream energy resources in the Ría de Muros (NW Spain). Renew Energy 2009;34:1517–24.
[67] Goss ZL, Coles DS, Kramer SC, Piggott MD. Efficient economic optimisation of large-scale tidal stream arrays. Appl Energy 2021;295:116975.

[68] Santa Catarina A. Wind power generation in Brazil: an overview about investment and scale analysis in 758 projects using the Levelized Cost of Energy. Energy Pol 2022;164:112830.
[69] Shields M, Beiter P, Nunemaker J, Cooperman A, Duffy P. Impacts of turbine and plant upsizing on the levelized cost of energy for offshore wind. Appl Energy 2021; 298:117189.
[70] Low WZ, vanden Broucke SKLM, Wynn MT, ter Hofstede AHM, De Weerdt J, van der Aalst WMP. Revising history for cost-informed process improvement. Computing 2016;98:895–921.
[71] Vazquez A, Iglesias G. Grid parity in tidal stream energy projects: an assessment of financial, technological and economic LCOE input parameters. Technol Forecast Soc Change 2016;104:89–101.
[72] Núñez L, López A, Somolinos J, Robledo F, Espín M. Methodologies for Tidal Energies Converters evaluation on early project phases. 2014.
[73] Hudson B, Kay E, Lawless M, Bruce T. Advanced metocean planning tools for the wave and tidal energy sectors. 2017.
[74] Martini M, Guanche R, Losada-Campa I, Losada IJ. The impact of downtime over the long-term energy yield of a floating wind farm. Renew Energy 2018;117:1–11.
[75] Obdam T, Braam H, René Van DP, Rademakers L. O&M cost estimation & feedback of operational data. In: Suvire Gastón O, editor. Wind farm. Rijeka: IntechOpen; 2011. Ch. 2.
[76] O'Connor M, Lewis T, Dalton G. Operational expenditure costs for wave energy projects and impacts on financial returns. Renew Energy 2013;50:1119–31.
[77] RealTide Consortium. RealTide deliverable D1.2 - RAM assessment report. Bureau Veritas; 2020. D1.2.
[78] Ernst Y. Cost of a financial support for wave, tidal stream and tidal range generation in the UK. A report for the Department of Energy and Climate Change and the Scottish Government; 2010.
[79] Ernst Y. Impact of banding the renewables obligation: costs of electricity production. Prepared by ernst and young. Commisioned by Department of Trade and Industry (DTI); 2007.